Aggressive Vehicle Control Using Polynomial Spiral Curves

Assylbek Dakibay*, Steven L. Waslander†

Abstract— **Autonomous driving at the limits of friction is not only a concept for racing autonomous cars but also a reliable method for emergency evasive manoeuvres in bad weather conditions. In this paper we introduce a method of incorporating smooth trajectory planner with an aggressive driving controller to implement double lane change manoeuvre while driving at the limits of tire friction**

I. INTRODUCTION

Aggressive vehicle control is an essential component of autonomous driving systems, as it enables maximum utilization of vehicle capabilities when required. In emergency evasive maneuvers, the ability to improve traction control through knowledge of the planned trajectory will lead to fewer accidents and a stronger safety case for full-vehicle autonomy. Although driving at high speeds is not the purpose of the autonomous driving technology, different weather conditions may affect the road quality in such a way as to dramatically reduce the friction limits and consequently the maximum safe velocity limits for vehicles.

A rich literature exists on vehicle controllers that has been developed for autonomous driving, ranging from methods that use Model Predictive Control techniques, [1], [2] to ones that utilize vehicle kinematics and dynamics to directly perform position tracking [3] [4]. Most of them do not deal with the problem of driving at the limits of friction. In [5] and [6], aggressive driving controllers are introduced that allow the autonomous vehicle to drive at the friction limit and maintain feasible path and velocity tracking. However, the tire model used in [6] and [5] assumes no longitudinal force is being applied at the front wheels, therefore making these methods only feasible for rear wheel drive vehicles. Most of the urban autonomous driving has been demonstrated at low speeds and in environments that do not include snowy or icy roads [7] [8]. Since the majority of passenger cars are front wheel drive, we propose an aggressive driving controller for Dugoff tire models, which incorporate longitudinal and lateral tire dynamics to accommodate front wheel drive vehicles.

Choosing and implementing any type of controller, however, affects the entire software architecture and especially the path and trajectory planner in an autonomous driving system. Autonomous driving systems employ complex software architecture that must be streamlined for computational efficiency and robust performance. Every element of the software system must have seamless integration with the rest of the modules and clear functional separation must exist between them to avoid overlapping tasks and to improve system performance [9], [10]. Although model predictive control methods are well established [6], it can be argued that vehicle trajectory planning and vehicle control should be separated for modularity and functional efficiency. A simple geometrical controller can be implemented with trajectory planner that uses dynamic vehicle model and vice versa [11], but planning and control must operate consistently so that plans generated are feasible for the controller to implement. As a result, since aggressive driving may require a controller that employs a dynamic vehicle model, the trajectory planner should also be based on the geometry of nonholonomic motion enforced by the underlying dynamics.

Some of the most popular methods for nonholonomic path planning in cluttered environments are based on using Dubins curves [12] and propose multiple variations of the path planning algorithm offered in [13]. The resulting path is a combination of constant radius curves and straight segments that can be refined by trajectory planner for continuous final curvature and more natural steering input. Although various trajectory planning methods exist for car-like robots, the aggressive driving controller requires the planner to provide the path curvature for velocity profile generation due to constraints that curvature imposes on the maximum driveable speed. In other words, to drive the vehicle at the tire force limits, the curvature profile must be available to the controller to generate the velocity profile that guarantees stability. The two most popular types of curves that are used to generate admissible trajectories for car-like robots using curvature profile are clothoids and polynomial spirals. Clothoids are curves with a linear curvature function, whereas polynomial spirals have n^{th} degree polynomial curvature profile [14].

In [5], an aggressive driving controller was implemented using a clothoids as path representation. However, the two available parameters of the clothoid are insufficient to generate a path with any arbitrary final heading or position, and therefore any maneuver such as a lane change or a turn must consist of several clothoid

† M.A.Sc. Candidate, Mechanical and Mechatronics Engineering, University of Waterloo; adakibay@uwaterloo.ca

‡ Associate Professor, Mechanical and Mechatronics Engineering, University of Waterloo; stevenw@uwaterloo.ca

978-1-5386-1526-3/17/$31.00 ©2017 IEEE

segments stitched together. In [15], bi-elementary simple clothoid paths were used for lane change maneuvers at the limits of friction. The bi-elementary clothoids are symmetrical configurations of clothoid segments with two constant curvature arcs joined by a straight segment. Note that symmetric bi-elementary clothoid paths can only be used to generate maneuvers with a final heading angle that is equal to the initial, severely limiting the path search space. Further, clothoids can not have second order continuity at the point of junction of two segments since the curvature is a first order linear function. Since the curvature has a direct effect on the steering wheel angle, the smoothness of the curvature profile ensures ride comfort and more natural steering angle dynamics. Nth-order polynomial spirals overcome all of the shortcomings of clothoids by being differentiable N-1 times, leading to a smoother curvature profile and a larger number of parameters that can be used to achieve any final configuration.

In [16] a polynomial spiral method is proposed for nonholonomic motion planning of planetary rovers. The curvature is selected to be a 3rd order polynomial. The coefficients of the polynomial are used as parameters for optimization to achieve the desired final position, heading and to match a higher level planner path. A method proposed in [17] showed that polynomial spirals can be used for obstacle avoidance along a known center line by generating a set of admissible curves with different offset distances and one is chosen using optimization that satisfies minimum curvature and is obstacle-free. In [18] a state lattice technique was introduced that allows for local obstacle avoidance using pre-planned polynomial spiral segments that can be joined after a discrete search finds the best configuration. Polynomial spirals, therefore, can be used for autonomous driving due to smooth curvature profile that guarantee more comfortable ride compared to clothoids and can be implemented with aggressive driving controller to keeping the vehicle within limits of friction when the road conditions deteriorate.

This paper proposes an aggressive driving controller to follow paths represented by polynomial spiral curves. The use of polynomial spiral paths allows for minimum jerk trajectories and smooth steering inputs, whereas the aggressive driving controller maintains the vehicle at the limits of tire friction and guarantees stable position and velocity tracking in extreme maneuvers. Our approach first generates a velocity profile to execute along the desired path by maximizing lateral forces at curvature maxima up to velocity limits, and then ensures longitudinal forces do not exceed friction limits. To ensure the controller takes into account longitudinal and lateral tire forces properly at the limits of friction, the Dugoff tire model is used throughout. We implement the results using CarSim, and demonstration both arbitrary paths with highly varying curvatures, and an evasive double lane-change maneuver for a front wheel drive sedan.

II. Problem Formulation

The trajectory planning method described in [16] generates the optimal path from an initial vehicle state $x_{in} = (x, y, \theta) \in \mathbb{R}^3$ to a desired state x_{des}. The vehicle desired path $\boldsymbol{x} = (x, y, \theta, \kappa)$ consists of a position x and y, heading angle θ and path curvature κ. Each component of the path, including the curvature profile, is paramaterized along the arc length s. The curvature is chosen to be represented by a cubic polynomial function $\kappa(s) : \mathbb{R} \to \mathbb{R}$. The four polynomial coefficients (a, b, c, d) and final arc length s_f of the curvature profile $\kappa(s)$ are used as optimization parameters (1) in generating the desired path.

$$\kappa(s) = a + bs + cs^2 + ds^3 \tag{1}$$

The curvature profile can be re-parameterized using knots, $\boldsymbol{p}$, that lie equidistantly along the length of the path [18], as defined in Equation (2).

$$\boldsymbol{p} = \begin{pmatrix} p_1 \\ p_2 \\ p_3 \\ p_4 \end{pmatrix} = \begin{pmatrix} \kappa(\frac{s_f}{3}) \\ \kappa(\frac{2s_f}{3}) \\ \kappa(s_f) \\ s_f \end{pmatrix} \tag{2}$$

The path components $(x(s), y(s), \theta(s))$ are generated by integrating the curvature to get the heading and integrating the heading to get the euclidean position as shown in Equation (3).

$$\begin{aligned} x(s) &= x_0 + \int_0^{s_f} cos(\theta(s))ds \\ y(s) &= y_0 + \int_0^{s_f} sin(\theta(s))ds \\ \theta(s) &= \theta_0 + \int_0^{s_f} \kappa(s)ds \end{aligned} \tag{3}$$

The position integral in this case is known as the Fresnel Integral and only has a numerical solution. In [16], a quadrature rule was proposed for calculating the integral and generating the path.

The path planner can be defined as a nonlinear optimization process subject to multiple constraints. The objective function for the optimization can vary depending on the design of the planner and desired behavior. The optimization is constrained by the the maximum and minimum curvature bounds that represent maximum vehicle steering angle and by desired final position, heading and curvature. If the optimization parameters can be denoted as $\boldsymbol{p} = (\ p_1 \quad p_2 \quad p_3 \quad s_f\ )$, then the constraint function $\boldsymbol{g}(p)$ can be expressed using boundary condition $\boldsymbol{h}(\boldsymbol{p})$ as shown in Equation (4):

$$\boldsymbol{g}(p) = \boldsymbol{h}(p) - \boldsymbol{x_f} = 0 \tag{4}$$

To find the smooth path from initial state $\boldsymbol{x_{in}}$ to final state $\boldsymbol{x_f}$ with upper and lower boundaries of the curvatures defined by $\pm\kappa_{max}$ the following optimization problem needs to be solved

$$\begin{aligned} \boldsymbol{min} \qquad & J = \tfrac{1}{2}\textstyle\int_0^{s_f} \kappa(p)^2 \\ s.t. \qquad & \boldsymbol{g}(p) = \boldsymbol{h}(p) - x_f = 0 \\ & -\kappa_{max} \leq \boldsymbol{p} \leq \kappa_{max} \end{aligned} \tag{5}$$

This basic formulation of the path planner optimization can be extended to include static and dynamic obstacle constraints, and can be integrated into heirarchical motion planners [11].

A. Velocity Profile

Once the path planner generates a curvature profile $k(s)$ and path to the desired final state $(x(s), y(s), \theta(s))$ the controller must execute it with minimum tracking error. It will be assumed the controller aims to drive the vehicle at the maximum possible velocity, given the desired path is chosen as was done in [7] and [18].

Velocity profile generation is based on the slip circle. The longitudinal $a_x(s)$ and lateral $a_y(s)$ acceleration along the path must be bounded by the friction limit of the road which is expressed as product of gravitational force g and coefficient of friction μ(6).

$$(\mu \cdot g)^2 = a_x(s)^2 + a_y(s)^2 \tag{6}$$

At the maximum point of the curvature, the longitudinal acceleration is set to zero and the vehicle corners at a constant velocity. Assuming steady state cornering the maximum velocity is found from acceleration which is proportional to radius $r(s)$ and square of longitudinal velocity $u_x(s)$ (7).

$$\mu \cdot g = a_y(s) \approx \frac{u_x(s)^2}{r(s)} \approx k(s) u_x(s)^2 \tag{7}$$

In the path segments preceding the maxima and following the maxima, however, the longitudinal acceleration does not need to be constrained to zero. Instead, the longitudinal acceleration can be expressed as a function of velocity, as follows.

$$a_x(s) = \frac{du_x}{dt} = \frac{du_x(s)}{ds} \cdot \frac{ds}{dt} = \frac{du_x(s)}{ds} \cdot u_x(s) \tag{8}$$

Therefore, the velocity profile can be found from Equation (9), which is a nonlinear differential equation.

$$\left(\frac{du_x(s)}{ds} \cdot u_x(s) \right)^2 = (\mu \cdot g)^2 - k(s)^2 \cdot u_x(s)^4 \tag{9}$$

The left hand side of Equation (9) can be rearranged using forward differencing. The velocity at the current path segment is expressed as u_s and $u_{s+\triangle s}$ is the velocity at distance $\triangle s$ along the curve (10).

$$\frac{du_x(s)}{ds} \cdot u_x(s) \approx \frac{\triangle u_x(s)}{\triangle s} \cdot u_x(s) = \frac{u_{s+\triangle s} - u_s}{\triangle s} \cdot u_s \tag{10}$$

The right hand side of Equation 9 represents the available longitudinal acceleration at a given point on the curve with the current curvature. When moving from the maximum curvature segment towards the lower curvature segment the vehicle should be able to accelerate but within the boundaries of the curvature of the next segment. Therefore an allowable acceleration and velocity must be found such that they do not violate the slip circle in (9). By using the numeric approximation in (10) and assuming we start at the point of maximum curvature the following equation can be used for generating the velocity profile.

$$U_s \cdot \frac{U_{s+\triangle s} - U_s}{\triangle s} = \sqrt{(\mu \cdot g)^2 - k_{s+\triangle s}^2 \cdot U_s^4} \tag{11}$$

where $k_{s+\triangle s}$ is the curvature at the new path segment and U_s is the velocity at the previous step. Solving for $U_{s+\triangle s}$ results in,

$$U_{s+\triangle s} = U_s \pm \triangle s \cdot \frac{\sqrt{(\mu \cdot g)^2 - k_{s+\triangle s}^2 \cdot U_s^4}}{U_s} \tag{12}$$

The terms under the square root represent the available longitudinal acceleration if the vehicle was to travel at the previous speed on a new segment with a smaller curvature $k_{s+\triangle s}$. Depending on the requirement, the allowable longitudinal acceleration is either added or subtracted from the initial velocity.

The resulting velocity profile can be used to calculate the maximum allowable acceleration profile for a given curvature profile using Equation 9. In order for the velocity profile planner to decide whether the obstacle avoidance maneuver should be performed with acceleration or deceleration, two profiles can be generated as two boundaries for possible velocity profiles. For braking, the given numeric approximation can be done until $U_{s+\triangle s}$ reaches zero - full stop. Since at every step the velocity is decreasing and no risk of violating the slip circle will occur even if the curvature is increasing, the profile generation for braking doesn't require a reverse integration step. If the calculation starts at the peak curvature then at every step the velocity profile will generate the maximum possible velocity with an acceleration that doesn't violate the slip circle or at the current velocity if the algorithm is run at real time. The polynomial spirals however can have up to two maximas and up to three different zeros and since the velocity only depends

on the magnitude of the curvature finding the maximas and minimas of $|k(s)|$ would require a search through the polynomial in the domain of interest. To generate the maximum velocity profile forward and backward integration must be performed using (12). An algorithm for velocity profile generation can be summarized below 1:

Algorithm 1 Velocity profile generation

Input: $\boldsymbol{p} = (\ p_1 \quad p_2 \quad p_3 \quad s_f\ )$ (curvature polynomial parameters), $\triangle s$ step size
forward integration
$N = \frac{s_f}{\triangle s}$ size of the path vector
for $i = 1 : N$ **do**
  if $(\mu \cdot g)^2 > k_{i+1}^2 \cdot u_i^4$ **then**
    $u_{i+1} = u_i + \triangle s \cdot \frac{\sqrt{(\mu \cdot g)^2 - k_{i+1}^2 \cdot u(i)^4}}{u(i)}$
  else $u_{i+1} = \sqrt{\frac{\mu \cdot g}{k_{i+1}}}$
  end if
end for
reverse integration
for $i = N : 1$ **do**
  if $(\mu \cdot g)^2 > k_{i-1}^2 \cdot u_i^4$ **then**
    $u_{i-1} = u_i + \triangle s \cdot \frac{\sqrt{(\mu \cdot g)^2 - k_{i-1}^2 \cdot u(i)^4}}{u(i)}$
  else $u_{i-1} = \sqrt{\frac{\mu \cdot g}{k_{i-1}}}$
  end if
end for
Output: velocity profile u_i, acceleration profile a_i

The velocity planning method addressed in [5] is only developed for simple clothoid segments, whereas the Algorithm 1 can be used for any type of curvature: defined discretely or as a continuous function. Even functions with irregular curvatures, such as B-splines, can be used for motion planning if the above-mentioned velocity generation profile method is chosen for aggressive driving applications.

B. Vehicle Model

The aggressive driving controller needs to use a dynamic vehicle model that captures the effect of tire forces and the effect of tire slip. Planar bicycle mode offers the framework for connecting the the tire dynamics to vehicle motion. The forces F_x, F_y acting on the vehicle can be summarized using vehicle mass m_v, front and rear tire forces F_{i_j}, distances from front axle a and rear axle b to the center of gravity of the vehicle,yaw rate $\dot{\theta}$ and moment of inertia about z axis I_{zz} as can be seen below:

$$\begin{aligned} F_x &= m_v \dot{y}\dot{\theta} + 2F_{x_f} + 2F_{x_r} \\ F_y &= -m_v \dot{x}\dot{\theta} + 2F_{y_f} + 2F_{y_r} \\ I_{zz}\ddot{\theta} &= 2aF_{y_f} - 2bF_{y_r} \end{aligned} \tag{13}$$

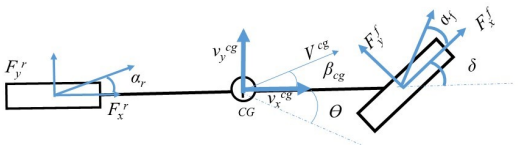

Fig. 1. Bicycle Model

The forces that tires generate can be expressed as a linear function of slip ratio for longitudinal tire force and slip angle for lateral tire force. The slopes of lateral and longitudinal tire forces, or longitudinal and lateral tire stiffness's, for a given vertical load, are assumed to constant within the linear tire region. From the tire curves the peak values for slip angle and slip ratio represent the point beyond which the the tire forces no longer behave linearly. It is important, therefore, that the vehicle stays within the linear tire region to maintain stability and ensure safety. The tire stiffness coefficient do not remain the same in the presence of combined slip. The Dugoff tire model captures the effect of combined slip by scaling down the longitudinal C_l and lateral C_r tire stiffness coefficients by the amount of longitudinal slip ration ζ and lateral slip angle α as can be observed in Equation (14).

$$\begin{aligned} F_x &= C_l \tfrac{\zeta}{1+\zeta} f(\lambda) \\ F_y &= C_r \tfrac{tan(\alpha)}{1+\zeta} f(\lambda) \\ \lambda &= \tfrac{\mu F_z (1+\zeta)}{2\sqrt{(C_l\zeta)^2 + (C_r tan(\alpha))^2}} \\ f(\lambda) &= (2-\lambda)\lambda \qquad if \quad \lambda < 1 \\ f(\lambda) &= 1 \qquad if \quad \lambda \geq 1 \end{aligned} \tag{14}$$

Front axle vertical load force F_z varies due to acceleration/deceleration induced pitch about the center of gravity of the vehicle and can be found from Equation (15)

$$F_{zf} = \frac{m_v(bg - ha_x m_v)}{a+b} \tag{15}$$

The parameter h is the height of the center of gravity.

C. Steering Controller

The steering controller is adopted from [19] and is based on generating desired lateral control force F_y. The desired lateral force F_y consists of two components F_y^{fb} feedback steering force and feedforward lateral force F_y^{ffd} as defined in Equation (16).

$$F_y = F_y^{fb} + F_y^{ffd} \tag{16}$$

The feedback force is calculated using artificial potential field that prevents the vehicle from deviating away from the centreline as described in [20]. The feedback force is calculated using crosstrack error e_{lat}, heading error

$\triangle\theta$, proportional gain k_{LK}, look ahead distance x_{la} and damping gain k_d.

$$F_y^{fb} = -k_{LK}(e_{lat} + x_{la} sin(\triangle\theta)) - k_d \triangle\dot{\theta} \quad (17)$$

The feedforward lateral force F_y^{ffd} mimics the behavior of the racing driver by turning ahead of the corner for better stability. Feedforward force is calculated at the front axle, where the effect of rear lateral force and moment forces generated from the rear tires about the center of gravity of the car are canceled out [19]. The effect of road curvature k and vehicle speed $\dot{s}$ and acceleration along the path $\ddot{s}$ is canceled out with feedforward force.

$$F_y^{ffwd} = \frac{m_v b}{a+b}(u_x k\dot{s} + x_{cop}(k\ddot{s} + \dot{k}\dot{s})) \quad (18)$$

Once the total desired lateral force is found, the desired front tire slip angle can be calculated using the Dugoff model. From the kinematics of the bicycle model, the steering wheel angle can be expressed as (19)

$$\delta = \frac{u_y + a\dot{\theta}}{u_x} - \alpha^{des}; \quad (19)$$

Using the slip angle derived from Dugoff model - desired steering angle δ can be calculated from 19.

D. Longitudinal Controller

The longitudinal controller finds the desired tracking velocity from the velocity profile and the vehicle position. Due to actuation delays and dynamic response of the vehicle tires, the longitudinal controller in [5] uses lookahead distance combined with proportional and integral gain terms for velocity profile tracking. Although the vehicle is intended to drive at the limits of friction, introducing the integral gain term for velocity tracking may keep increasing the feedback command even when the tire force is saturated. The controller, therefore, might become unstable over time. The final longitudinal force command, F_x^{cmd}, is calculated by summing multiple force components (20), as follows,

$$F_x^{cmd} = F^V + F_x^{slip} + F_D \quad (20)$$

The resistance force, F_D, consists of multiple terms that summarize the sources of resistance acting on a vehicle 21.

$$F_D = F_r + F_a + F_g + F_c \quad (21)$$

where F_a is the aerodynamic , F_r is the rolling resistance that can be estimated for each vehicle using coast downhill test, F_g is the force due to road grade angle θ_g and F_c is the longitudinal force component due to front axle steering angle during cornering. The speed tracking force, F^V, is calculated using a proportional gain K_v and

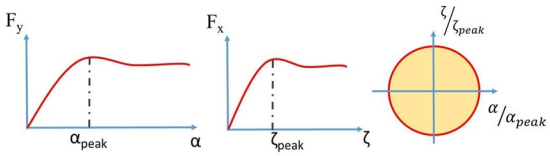

Fig. 2. Tire Force Curves and g-g Diagram

velocity error between the vehicle speed V_x and desired speed from the velocity profile V_{des} 22

$$F^V = K_v(V_{des} - V_x) \quad (22)$$

The slip circle is the representation of the available tire force during combined lateral and longitudinal slipping. The slip circle allows the controller to identify the available longitudinal force when the vehicle is cornering at peak forces. The purpose of using the slip circle feedback is not to make the vehicle drift, but rather to keep it just within the friction limit of the tire. The slip circle feedback force F_x^{slip} is calculated using the normalized slip circle diagram technique proposed in [5]. Two axes of the slip circle are the longitudinal slip ratio and lateral slip angle normalized by the peak values based on the tire force curve (23)

$$\bar{\alpha} = \frac{\alpha}{\alpha_{peak}}$$
$$\bar{\zeta} = \frac{\zeta}{\zeta peak} \quad (23)$$

The slip circle feedback force F_x^{slip} is only implemented on the longitudinal controller to make sure the steering controller always has maximum available lateral force to keep the vehicle on the path and can be summarized in the following equation (24):

$$F_x^{slip} = \begin{cases} K_\zeta \triangle\bar{\zeta} + K_\alpha \triangle\bar{\alpha}, & \bar{\zeta} \leq 0 \\ -K_\zeta \triangle\bar{\zeta} - K_\alpha \triangle\bar{\alpha}, & \bar{\zeta} > 0 \end{cases} \quad (24)$$

The slip circle feedback force is proportional to the normalized distances to the edge of the slip circle along the slip angle $\bar{\alpha}$ and slip ratio $\bar{\zeta}$ axes with associated proportional gains K_κ and K_α. The distances $\triangle\bar{\alpha}$ and $\triangle\bar{\kappa}$ are calculated such that the vehicle uses most of the available longitudinal force to reach the edge of the slip circle when lateral slip angle is less than the peak force. When the tire comes close to saturating the lateral force the remaining available force is used to bring the tire back to the edge of the slip circle, as defined in Equations (25) and (26).

$$\triangle\bar{\kappa} = \begin{cases} |\bar{\zeta}| - \sqrt{1-\bar{\alpha}^2}, & \bar{\alpha} \leq 1 \\ |\bar{\zeta}|, & \alpha > 1 \end{cases} \quad (25)$$

$$\triangle\bar{\alpha} = \begin{cases} 0, & \bar{\alpha} \leq 1 \\ |\bar{\alpha}| - 1, & \bar{\alpha} > 1 \end{cases} \quad (26)$$

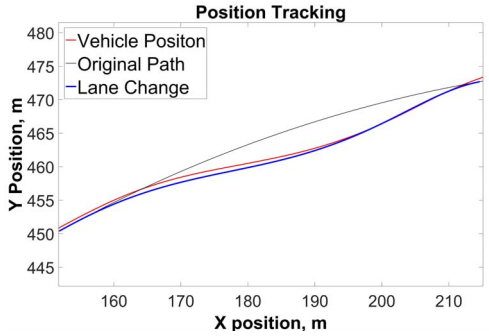

Fig. 3. Position Tracking

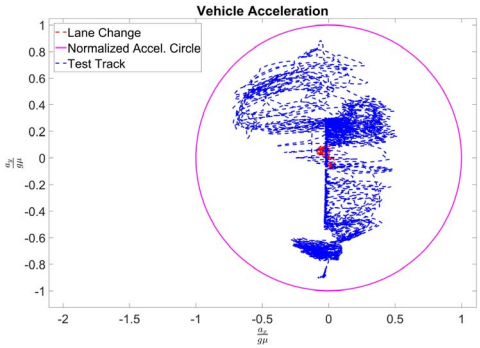

Fig. 4. Acceleration against slip circle

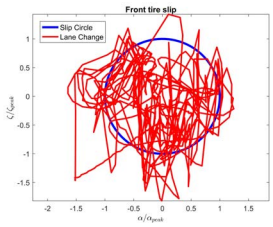

Fig. 5. g-g diagram and tire slip

The final longitudinal force as proposed in [5] is converted into desired throttle or brake pedal signal using engine and brake torque maps. While using full longitudinal control force F_x can be feasible for rear wheel drive vehicle, for front wheel drive cars additional measures need to be taken to prevent the vehicle from losing traction due to combined slip. The total control force during the combined slip can be compared to the available longitudinal force from Dugoff model F_x^{Dm} in Equation (14) and the smallest of the two should be chosen as oppose to the method described in [5], which doesn't check for the available longitudinal force and the method in [21], which assumes constant front load.

$$F_x = min(F_x^{Dm}, F_x^{cmd}) \tag{27}$$

III. Simulation Results

The simulation was implemented on high fidelity vehicle simulation software CarSim. To demonstrate the capabilities of the polynomial spirals a smooth double lane change maneuver is implemented from a single set of parameters while the vehicle is already driving at top available speed along a larger polynomial spiral segment at maximum speed. The position tracking results for lane change maneuver had largest cross track error of 0.7m at the entry to the lane change curve and less than 0.01 m towards the exit as can be observed in Figure 3 and Figure 7. The heading error stays within 0.04 radians. While having feasible position tracking the controller also keeps the vehicle within the road friction limits. In Figure 4 the vehicle acceleration is plotted with a circle of radius equal to road friction capacity μg, vehicle stays with the circle during reference path following as well as during lane change. The front tire average slip shown on the g-g diagram in Figure 5 stays in the vicinity of the unit circle on the lateral slip angle axis $\frac{\alpha}{\alpha_{peak}}$ since the longitudinal controller gives preference to having maximum lateral force available for stable steering. On the longitudinal slip axis $\frac{\zeta}{\zeta_{peak}}$, however, the slip ratio leaves the circle while acceleration as well as braking. One of the reasons for this the look ahead distance on the feedback controller that keeps the vehicle speed at an offset from the velocity profile and therefore vehicle ends up being above the allowable vehicle speed limit as can be seen fro Figure 6. Overall velocity tracking performance keeps the vehicle at the maximum possible speed while implementing reliable position tracking

IV. CONCLUSIONS

Implementing aggressive driving controller provides the necessary safety oriented trajectory planning and tracking framework that can be used for emergency evasive maneuvers during poor road conditions as well as for autonomous driving on low friction surfaces such as gravel, mud and ice. The aggressive driving controller implemented with smooth curvature polynomial spiral is guaranteed to keep the vehicle within friction limits by generating maximum safe velocity profile and using the

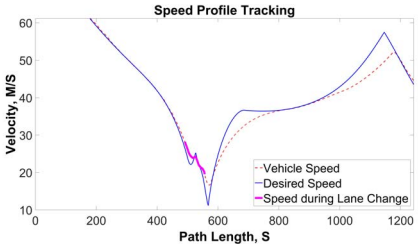

Fig. 6. Velocity Tracking

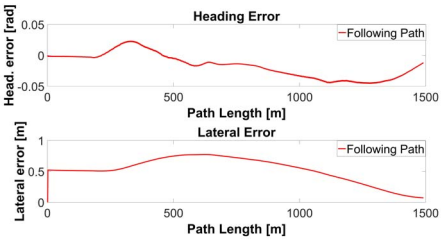

Fig. 7. Tracking Error

g-g diagram for keeping the tire forces within safe region of operation.

ACKNOWLEDGMENT

REFERENCES

[1] L. Ni, A. Gupta, P. Falcone, and L. Johannesson, "Vehicle lateral motion control with performance and safety guarantees," *IFAC-PapersOnLine*, vol. 49, no. 11, pp. 285–290, 2016.

[2] F. Borrelli, P. Falcone, T. Keviczky, J. Asgari, and D. Hrovat, "Mpc-based approach to active steering for autonomous vehicle systems," *International Journal of Vehicle Autonomous Systems*, vol. 3, no. 2-4, pp. 265–291, 2005.

[3] R. C. Coulter, "Implementation of the pure pursuit path tracking algorithm," DTIC Document, Tech. Rep., 1992.

[4] B. d'Andréa Novel, G. Campion, and G. Bastin, "Control of nonholonomic wheeled mobile robots by state feedback linearization," *The International journal of robotics research*, vol. 14, no. 6, pp. 543–559, 1995.

[5] K. Kritayakirana and J. C. Gerdes, "Autonomous vehicle control at the limits of handling," *International Journal of Vehicle Autonomous Systems*, vol. 10, no. 4, pp. 271–296, 2012.

[6] M. Brown, J. Funke, S. Erlien, and J. C. Gerdes, "Safe driving envelopes for path tracking in autonomous vehicles," *Control Engineering Practice*, vol. 61, pp. 307–316, 2017.

[7] J. Ziegler, P. Bender, M. Schreiber, H. Lategahn, T. Strauss, C. Stiller, T. Dang, U. Franke, N. Appenrodt, C. G. Keller *et al.*, "Making bertha drivean autonomous journey on a historic route," *IEEE Intelligent Transportation Systems Magazine*, vol. 6, no. 2, pp. 8–20, 2014.

[8] M. Campbell, M. Egerstedt, J. P. How, and R. M. Murray, "Autonomous driving in urban environments: approaches, lessons and challenges," *Philosophical Transactions of the Royal Society of London A: Mathematical, Physical and Engineering Sciences*, vol. 368, no. 1928, pp. 4649–4672, 2010.

[9] S. Ulbrich, A. Reschka, J. Rieken, S. Ernst, G. Bagschik, F. Dierkes, M. Nolte, and M. Maurer, "Towards a functional system architecture for automated vehicles," *arXiv preprint arXiv:1703.08557*, 2017.

[10] Ö. Ş. Taş, F. Kuhnt, J. M. Zöllner, and C. Stiller, "Functional system architectures towards fully automated driving," in *Intelligent Vehicles Symposium (IV), 2016 IEEE*. IEEE, 2016, pp. 304–309.

[11] B. Paden, M. Čáp, S. Z. Yong, D. Yershov, and E. Frazzoli, "A survey of motion planning and control techniques for self-driving urban vehicles," *IEEE Transactions on Intelligent Vehicles*, vol. 1, no. 1, pp. 33–55, 2016.

[12] L. E. Dubins, "On curves of minimal length with a constraint on average curvature, and with prescribed initial and terminal positions and tangents," *American Journal of mathematics*, vol. 79, no. 3, pp. 497–516, 1957.

[13] J. Reeds and L. Shepp, "Optimal paths for a car that goes both forwards and backwards," *Pacific journal of mathematics*, vol. 145, no. 2, pp. 367–393, 1990.

[14] Y. J. Kanayama and B. I. Hartman, "Smooth local-path planning for autonomous vehicles1," *The International Journal of Robotics Research*, vol. 16, no. 3, pp. 263–284, 1997.

[15] J. Funke and J. C. Gerdes, "Simple clothoid paths for autonomous vehicle lane changes at the limits of handling," in *ASME 2013 dynamic systems and control conference*. American Society of Mechanical Engineers, 2013, pp. V003T47A003–V003T47A003.

[16] A. Kelly and B. Nagy, "Reactive Nonholonomic Trajectory Generation via Parametric Optimal Control," in *The International Journal of Robotics Research*, vol. 22, no. 7-8, 2003, pp. 583–601.

[17] T. M. Howard, C. J. Green, A. Kelly, and D. Ferguson, "State space sampling of feasible motions for high-performance mobile robot navigation in complex environments," *Journal of Field Robotics*, vol. 25, no. 6-7, pp. 325–345, 2008.

[18] M. Pivtoraiko and A. Kelly , "Efficient constrained path planning via search in state lattices," in *The 8th International Symposium on Artificial Intelligence, Robotics and Automation in Space*, Munich, Germany, September 2005.

[19] K. Kritayakirana and J. C. Gerdes, "Using the centre of percussion to design a steering controller for an autonomous race car," *Vehicle System Dynamics*, vol. 50, no. sup1, pp. 33–51, 2012.

[20] E. J. Rossetter, J. P. Switkes, and J. C. Gerdes, "Experimental validation of the potential field lanekeeping system," *International journal of automotive technology*, vol. 5, no. 2, pp. 95–108, 2004.

[21] S. Song, A. Wong, J. Huissoon, and S. L. Waslander, "Autonomous Vehicle Control Near the Limit of Friction," no. 2, pp. 1008–1013, 2015.